RESEARCH PAPER

Comparative Evaluation of Stress at the Implant–Bone Interface Between Zirconia and Titanium Implants with Different Occlusal Material: A Three-Dimensional Finite Element Analysis

Dr. Aaron G Baby[1], **Dr. Annapoorni Hariharan**[1*], **Dr. Shyam Sundar Shanker**[1], **Dr. Saishree Anchana R**[1], **Dr. Sushmita S**[1], **Dr. Devi Parameswari**[1]

[1*]Department of Prosthodontics and Crown and Bridge, Meenakshi Ammal Dental College and Hospital, Meenakshi Academy of Higher Education and Research (Deemed to be University), Chennai, Tamil Nadu, India

[1]Post Graduate Student (Dr. Aaron G Baby) | ORCID: https://orcid.org/0009-0007-7561-4778 | Email: aarongbaby6@gmail.com

[1*]Professor and Head of the Department (Dr. Annapoorni Hariharan) | ORCID: https://orcid.org/0000-0003-1175-5882 | Email: profhod.prostho@madch.eu.in

[1]Professor (Dr. Shyam Sundar Shanker) | ORCID: https://orcid.org/0000-0003-1019-2950 | Email: drshyam.prostho@gmail.com

[1]Post Graduate Student (Dr. Saishree Anchana R) | ORCID: https://orcid.org/0000-0002-5660-2938 | Email: saishreeanchana@gmail.com

[1]Post Graduate Student (Dr. Sushmita S) | ORCID: https://orcid.org/0009-0001-4595-919X | Email: sushmi25suja@gmail.com

[1]Professor (Dr. Devi Parameswari) | Email: drdeviparameswari@gmail.com

***Corresponding Author:** Dr. Annapoorni Hariharan, Professor and Head of the Department, Department of Prosthodontics and Crown and Bridge, Meenakshi Ammal Dental College and Hospital, Meenakshi Academy of Higher Education and Research (Deemed to be University), Chennai, Tamil Nadu, India | ORCID: https://orcid.org/0000-0003-1175-5882 | Email: profhod.prostho@madch.eu.in

Abstract

Background: Implant and restorative materials influence the biomechanical performance of implant-supported restorations. Objective: To compare stress distribution around titanium and zirconia implants restored with graphene or monolithic zirconia crowns using three-dimensional finite element analysis. Materials and Methods: Four finite element models (GTg, GTm, GZg and GZm) with standardized zirconia abutments were analyzed under axial and oblique loading. Maximum von Mises stresses were evaluated in the implant, abutment, retaining screw, crown, cortical bone and cancellous bone. Results: Stress was concentrated predominantly at the crestal module of the implant. Zirconia implants exhibited higher internal implant stresses, whereas titanium implants transferred relatively greater stress to the surrounding bone. Graphene crowns demonstrated a more favorable stress distribution than monolithic zirconia crowns. Oblique loading generated higher stresses than axial loading. Conclusion: Implant material, restorative material and loading direction significantly influence biomechanical behavior and should be considered during treatment planning

How to cite this article: Baby AG, Hariharan A, Shanker SS, Anchana R S, Sushmita S, Parameswari D. Comparative evaluation of stress at the implant–bone interface between zirconia and titanium implants with different occlusal material: a three-dimensional finite element analysis. Int J Drug Deliv Technol. 2026;16(75s): 68-84. DOI: 10.25258/ijddt.16.75s.8

Introduction

Dental implants have become a predictable and widely accepted treatment modality for replacing missing teeth, restoring function, esthetics, phonetics, and patient comfort. Advances in implant design, biomaterials, surgical protocols, and prosthetic rehabilitation have resulted in high long-term survival rates of implant-supported restorations.[1,2] However, biological and mechanical complications, including crestal bone loss, screw loosening, component fracture, and failure of osseointegration, continue to influence long-term success. Among the factors affecting implant longevity, stress transmission from the prosthesis to the implant and surrounding bone remains a critical determinant of peri-implant stability.[3,4]

Unlike natural teeth, which are supported by the periodontal ligament, dental implants are directly ankylosed to bone through osseointegration, resulting in direct transfer of occlusal forces to the peri-implant bone.[5] This often leads to stress concentration in the crestal cortical bone multiple factors, including implant material, bone quality, loading direction,and restorative material.[3,4]Titanium remains the gold standard for dental implants because of its excellent biocompatibility, corrosion resistance, and long-term clinical success.[6,7] However, the esthetic limitations of titanium and its high elastic modulus relative to bone have prompted the development of alternative materials such as zirconia. Zirconia offers favorable esthetics, biocompatibility, and corrosion resistance but exhibits distinct biomechanical behavior because of its greater stiffness.[8,9]Restorative material also plays an important role in load transfer. Monolithic zirconia crowns are widely used because of their strength and durability, whereas graphene-based restorative materials have recently attracted interest owing to their lower elastic modulus and potential to absorb and redistribute occlusal forces.[10,11] Although the biomechanical behavior of implant and restorative materials has been investigated independently, limited evidence is available regarding their combined influence on stress distribution within the implant-restoration complex.

Therefore, the present study aimed to compare the stress distribution in the implant, abutment, crown, and peri-implant bone of titanium and zirconia implants restored with monolithic zirconia and graphene crowns using three-dimensional finite element analysis.

Materials and Methods

Study design

A three-dimensional finite element analysis (FEA) was performed to compare stress distribution within the implant, peri-implant bone, abutment, retaining screw, and crown between titanium and zirconia implants restored with graphene and monolithic zirconia crowns. The analysis comprised three phases: pre-processing (model construction, material property assignment, meshing, and boundary condition application), processing (loading simulation), and post-processing (stress evaluation).

Finite element model construction

A three-dimensional mandibular first molar bone model representing Type I bone quality was designed using Blender 3D and SolidWorks CAD software. The model consisted of a 2-mm cortical bone layer surrounding cancellous bone, with overall dimensions of 15 mm × 25 mm.

A Straumann BLT Roxolid RC implant (4.1 × 14 mm) was scanned using a Bruker SkyScan 2214 micro-computed tomography scanner, and the images were reconstructed using NRecon software to generate a three-dimensional model. A Straumann cementable zirconia abutment (5.0 mm diameter, 5.5 mm height, 2 mm gingival height) and its retaining screw were reconstructed using the same protocol. Anatomically contoured mandibular first molar crowns were designed in SolidWorks according to Wheeler's Dental Anatomy. Two crown materials were evaluated: monolithic zirconia and graphene, each fabricated with a uniform thickness of 2 mm and a 0.8-mm shoulder finish line.

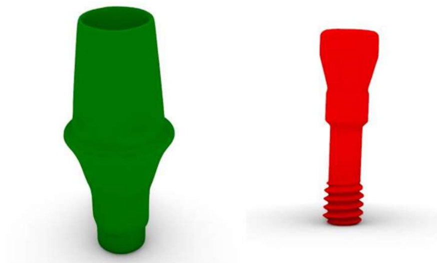

Figure 2.1: Implant fixture model
Figure 2.2: Model of abutment and retaining screw

Figure 2.3: Model of the crown

MESHING

To perform a detailed analysis with improved accuracy and to confirm the analysis results, a process called meshing is done. After the fabrication of 3 D finite element models, they were fed into ANSYS software and meshed (Figure 2. 4). This is done so that the stresses after loading can be measured in better clarity. All the materials used in the models were considered to be isotropic, linear and homogenous.

Figure 2.4: Models after meshing

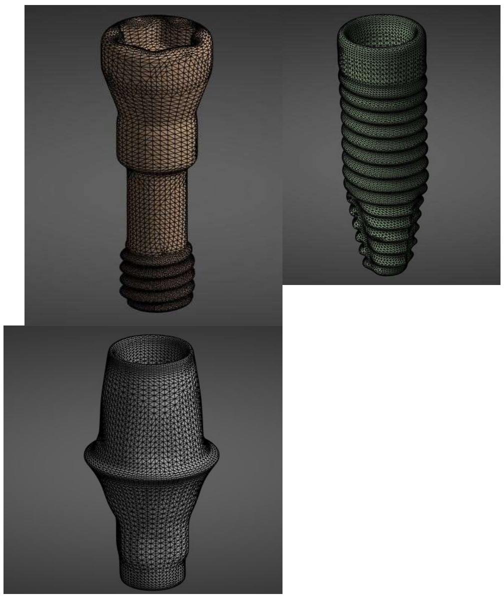

DATA FOR THE INDIVIDUAL MATERIAL PROPERTIES

Material properties that was used for the finite element model construction includes the Young's modulus and Poisson's ratio.

MATERIAL	YOUNGS'S MODULUS (GPa)	POISSON'S RATIO
ZIRCONIA CROWN	200	0.30
GRAPHENE CROWN	3.2	0.19
TITANIUM IMPLANT	113.8	0.34
ZIRCONIA IMPLANT	200	0.31
ZIRCONIA ABUTMENT	200	0.31

Table 1. 1 :Material properties of implant components

BONE	MODULUS OF ELASTICITY(Gpa)	POISSON'S RATIO
CORTICAL BONE	13.7	0.30
CANCELLOUS BONE	1.37	0.37

Table 1. 2: Material properties of bone components

ELEMENTS AND NODES FOR THE MODELS

Model	NODES	ELEMENTS
IMPLANT	122351	70155
ABUTMENT	77181	44603
SCREW	56146	32070
CROWN	62083	36302
CORTICAL	355054	208104
CANCELLOUS	66145	38394

Table 1.3: Nodes and elements of different components after meshing

ASSEMBLING THE FINITE ELEMENT MODEL:

The current study was divided into four groups (Figure 2.5):

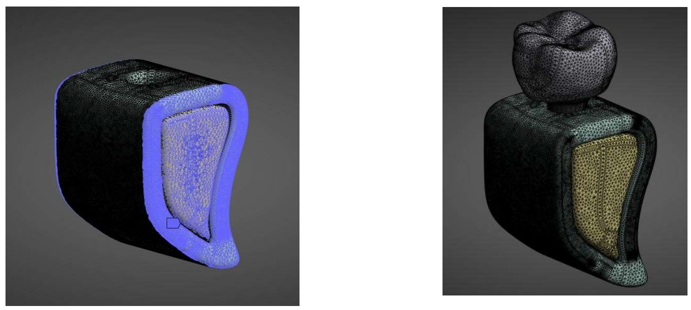

Figure 2.5: Sample groups

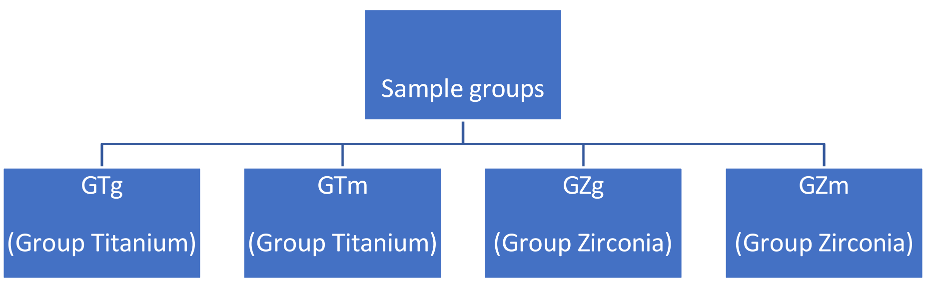

GTg – Titanium implant with graphene crown
GTm – Titanium implant with monolith zirconia crown GZg – Zirconia implant with graphene crown
GZm – Zirconia implant with monolith zirconia crown

Both the Zirconia and Titanium implant models with dimension of 4.1 ×14mm were fixed into the bone 1mm subcrest ally, at the centre of the mandibular crest. It is assumed that the bone -implant interface has tight contact and simulates ideal Osseo -integrated situations.

The crown is fixed over the abutment whose material was standardised as zirconia abutment for all groups and a tight contact between them is assumed. The thickness of the cement is not considered in the study (Figure 2.6).

BOUNDARY CONDITIONS

Boundary condition is an important parameter to perform any FEA analysis. The cut section of the mandibular molar region is arrested in all degrees of freedom (Figure 2.7).

Figure 2.6: Assembly model Figure 2.7: Boundary conditions

PROCESSING – LOADING PROTOCOL

The reality of loading is a combination of axial and oblique load. Hence in this study, this combination is considered as it will show the highest localised stress in the surrounding bone.

The crowns are subjected to two different loading conditions.

1. A distributed load of a maximum of 600N (maximum biting force) is applied in the axial direction at eight different loading points. A load of 75N is applied at 3 points on the outer and inner slopes of buccal cusps and at 2 points on the inner slopes of the lingual cusp. (Figure 2.8)
2. A distributed load of 225N at 0° horizontally, 45° non- axially, and 90 ° axially. For these, three loading points were selected on the outer slopes of buccal cusps and each point was subjected to 75N.

Figure 2.8 : Loading points – Three points on the inner slopes of buccal cusp and two points on the inner slopes of lingual cusps
marked in blue. Three points on outer slopes of buccal cusps marked in green

The regions where the stress will be studied in all the three groups are:

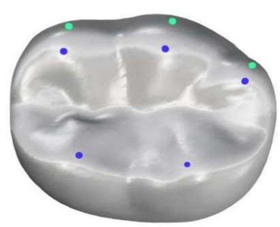

Bone, implant, abutment, screw and crown

POST PROCESSING

After loading, the maximum Von Misses stress values pertaining to the implant, bone, abutment and the retaining screws were evaluated. The various interpretations regarding the stress values can be visualised using different colour coding provided from blue (minimal stress) to red (maximum stress).

Results

In all figures, the top left model represents GTg (Group Titanium graphene), the top right model represents GTm (Group Titanium monolith zirconia), the bottom left model represents GZg (Group Zirconia graphene), and the bottom right model represents GZm (Group Zirconia monolith zirconia). The three - dimensional finite element analysis was carried out in four experim ental groups: GTg, GTm, GZg, and GZm. Stress distribution was assessed in the implant, abutment and screw, crown, cortical bone, and cancellous bone under one axial loading condition of 600 N and three oblique loading conditions of 225 N at 0°, 45°, and 90 °.

Von mises stress in the implant

Figure 3.1: Von misses stresses evaluated at the crestal module of implant under axial loading (600N)

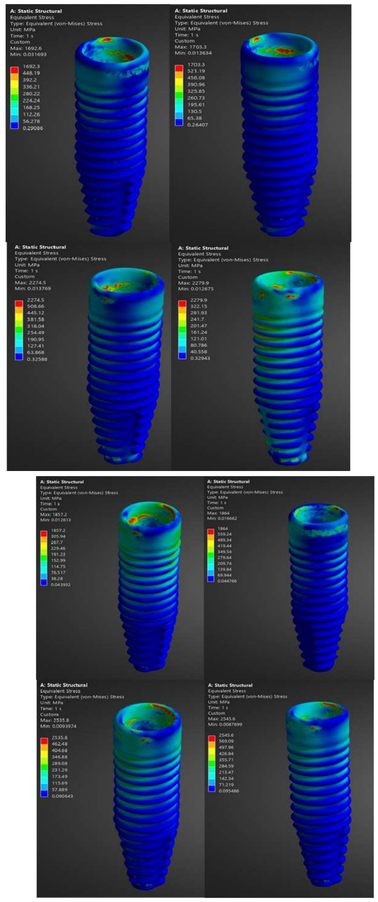

Under axial loading (600 N), von Mises stress was predominantly concentrated at the crestal module of the implant in all groups, particularly around the implant platform and coronal threads. The zirconia implant groups exhibited higher stress concentrations than the titanium groups, with GZm showing the highest stress (2279.9 MPa), followed by GZg (2274.5 MPa), GTm (1703.3 MPa), and GTg (1692.3 MPa). Irrespective of crown material, the crestal module remained the primary stress-bearing region under axial load.

Figure 3.2: Von misses stresses evaluated at the crestal module of implant under 0° oblique loading(225N)

Under 0° oblique loading (225 N), von Mises stress remained concentrated at the crestal module, with greater localization at the coronal portion of the implant compared with axial loading. Zirconia implant groups exhibited higher stress concentrations than titanium groups, with GZm demonstrating the highest stress (2545.6 MPa), followed by GZg (2535.8 MPa), GTm (1864.0 MPa), and GTg (1857.2 MPa). The crestal module remained the primary site of stress concentration irrespective of the crown material.

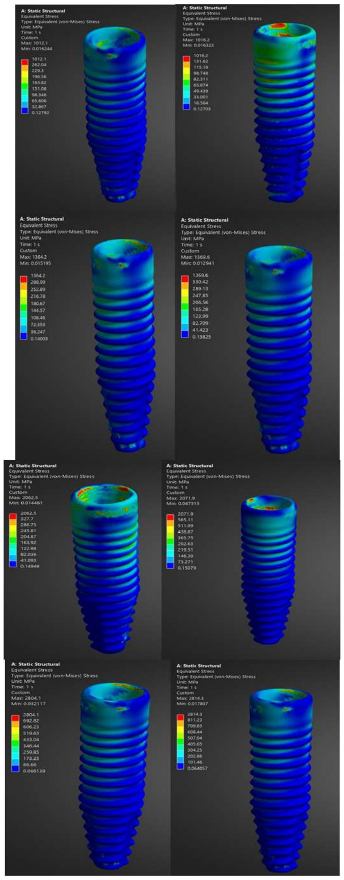

Figure 3.3: Von misses stresses evaluated at the crestal module of implant under 45° oblique loading(225N)

Under 45° oblique loading (225 N), von Mises stress further increased at the crestal module and was more intensely localized in the coronal region than under axial or 0° oblique loading. Zirconia implant groups demonstrated higher stress concentrations than titanium groups, with GZm exhibiting the highest stress (2814.3 MPa), followed by GZg (2804.1 MPa), GTm (2071.9 MPa), and GTg (2062.5 MPa). Among all loading conditions, 45° oblique loading produced the greatest stress concentration at the crestal module.

Figure 3.4: Von misses stresses evaluated at the crestal module of implant under 90° oblique loading(225N)

Under 90° oblique loading (225 N), von Mises stress remained concentrated at the crestal module, although the magnitude was lower than that observed under 45° oblique loading. Zirconia implant groups exhibited higher stress concentrations than titanium groups, with GZm demonstrating the highest stress (1369.6 MPa), followed by GZg (1364.2 MPa), GTm (1016.2 MPa), and GTg (1012.1 MPa). Despite the lower stress magnitude, the crestal module remained the principal site of stress concentration in all groups.

Overall, maximum von Mises stress was consistently concentrated at the crestal module under all loading conditions, with the highest stress observed during 45° oblique loading. The coronal portion of the implant remained the most biomechanically critical region irrespective of the crown or implant material.

Von mises stress in the abutment and screw

Figure 3.5: Von misses stresses at the abutment and screw under axial loading (600N)

Under axial loading (600 N), von Mises stress in the abutment-screw complex was predominantly concentrated in the cervical and middle third of the abutment. The highest stress was observed in GZm and GTm (1692.6 MPa each), followed by GTg (1424.9 MPa) and GZg (1422.5 MPa). The cervical region of the abutment represented the primary site of stress transfer within the implant-abutment complex.

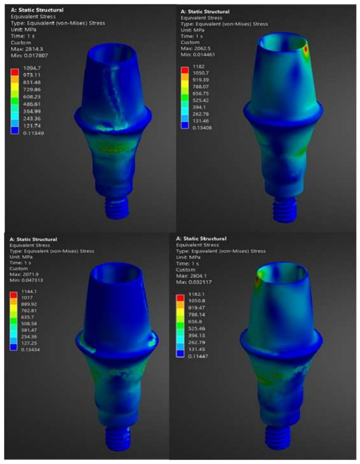

Figure 3.6: Von misses stresses at the abutment and screw under 0° oblique loading (225N)

Under 0° oblique loading (225 N), von Mises stress remained concentrated in the cervical region of the abutment. The highest stress was observed in GZm (1236.2 MPa), followed by GZg (1231.0 MPa), GTm (1104.4 MPa), and GTg (1104.4 MPa). Overall, the graphene crown groups exhibited lower stress concentrations within the abutment-screw complex than the monolithic zirconia crown groups.

Figure 3.7: Von misses stresses at the abutment and screw under 45° oblique loading (225N)

Under 45° oblique loading (225 N), von Mises stress remained concentrated in the cervical region of the abutment. The highest stress was observed in GTm (1182.1 MPa), closely followed by GZm (1182.0 MPa), GZg (1144.1 MPa), and GTg (1094.7 MPa). GTg demonstrated the lowest stress among all groups.

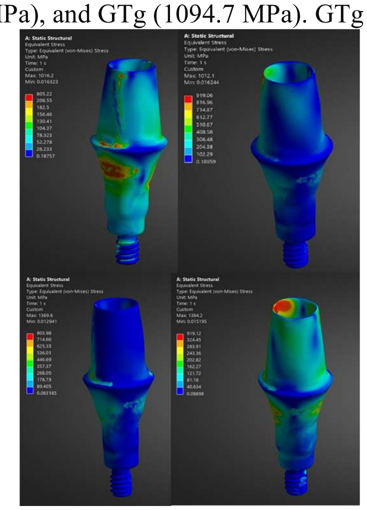

Figure 3.8: Von misses stresses at the abutment and screw under 90° oblique loading (225N)

Under 90° oblique loading (225 N), von Mises stress remained predominantly concentrated in the cervical region of the abutment. GZm exhibited the highest stress (919.12 MPa), closely followed by GTm (919.06 MPa), while GZg (803.98 MPa) and GTg (805.22 MPa) demonstrated lower and comparable stress values. The cervical region remained the principal site of stress concentration under this loading condition.

Overall, maximum von Mises stress within the abutment-screw complex was consistently concentrated in the cervical region under all loading conditions. The highest stress values were observed under axial loading, with stress decreasing under oblique loading. Since zirconia abutments were standardized across all groups, the variations in stress distribution can be attributed to differences in implant material, crown material, and loading direction rather than the abutment material itself.

Von mises stress in the crown

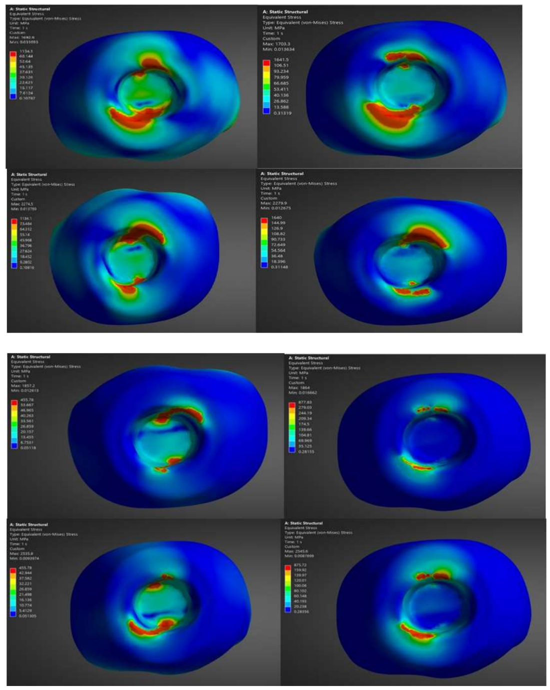

Figure 3.9: Von misses stresses on the crown under axial loading (600N)

Under axial loading (600 N), von Mises stress within the crown was highest in GTm (1641.5 MPa), followed closely by GZm (1640.0 MPa), while GZg (1136.1 MPa) and GTg (1134.1 MPa) exhibited lower stress values. Overall, the monolithic zirconia crown groups demonstrated higher crown stresses than the graphene crown groups under axial loading.

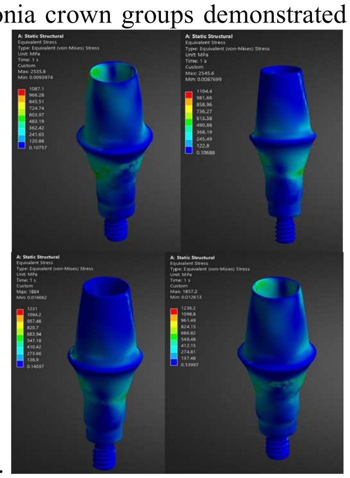

Figure 3.10: Von misses stresses on the crown under 0° oblique loading (225N)

Under 0° oblique loading (225 N), von Mises stress within the crown was highest in GTm (877.8 MPa), followed closely by GZm (875.7 MPa), while GTg and GZg exhibited lower and identical stress values

(455.7 MPa each). The monolithic zirconia crown groups consistently demonstrated higher crown stresses than the graphene crown groups.

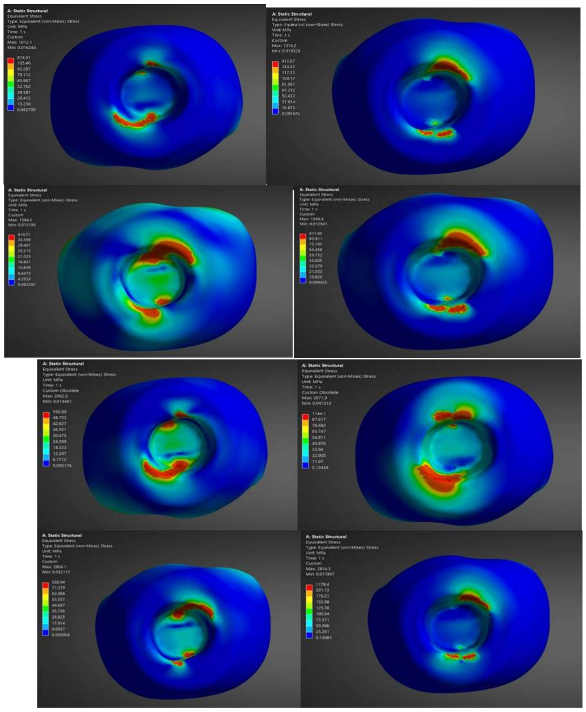

Figure 3.11: Von misses stresses on the crown under 45° oblique loading (225N)

Under 45° oblique loading (225 N), von Mises stress within the crown was highest in GZm (1178.4 MPa), followed by GTm (1144.1 MPa), while GTg and GZg exhibited lower and identical stress values (550.9 MPa each). Crown stress increased markedly under 45° oblique loading, particularly in the monolithic zirconia crow n groups.

Figure 3.12: Von misses stresses on the crown under 90° oblique loading (225N)

Under 90° oblique loading (225 N), von Mises stress within the crown was highest in GTm (912.8 MPa), followed closely by GZm (911.8 MPa), while GTg and GZg demonstrated lower and identical stress values (814.5 MPa each). The monolithic zirconia crown groups consistently exhibited higher crown stresses than the graphene crown groups under this loading condition.

Von mises stress in the cortical bone

Figure 3.13: Von misses stresses in the cortical bone under axial loading (600N)

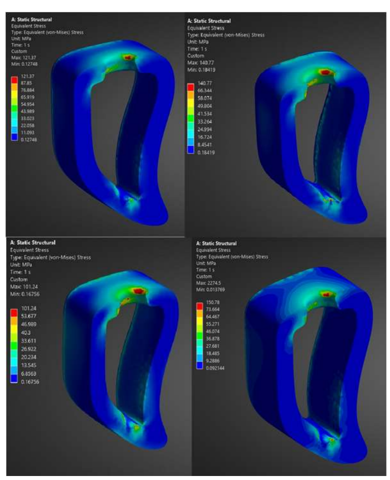

Under axial loading (600 N), von Mises stress within the cortical bone was predominantly concentrated in the crestal region adjacent to the implant neck. GZm exhibited the highest stress (150.78 MPa), followed by GTm (140.77 MPa), GTg (121.77 MPa), and GZg (101.24 MPa). The crestal cortical bone remained the primary site of stress transfer under axial loading.

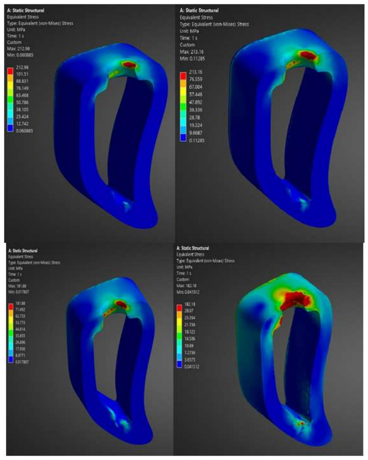

Figure 3.14: Von misses stresses in the cortical bone under 0° oblique loading (225N)

Under 0° oblique loading (225 N), von Mises stress within the cortical bone increased compared with axial loading. GTg exhibited the highest stress (247.68 MPa), followed closely by GTm (247.39 MPa), while GZm (214.22 MPa) and GZg (213.90 MPa) demonstrated lower and comparable stress values. Overall, the titanium implant groups exhibited slightly higher cortical bone stresses than the zirconia implant groups.

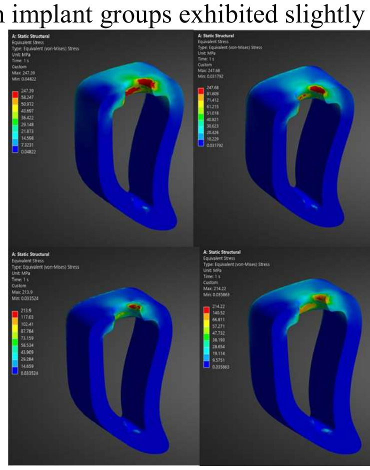

Figure 3.15: Von misses stresses in the cortical bone under 45° oblique loading (225N)

Under 45° oblique loading (225 N), the cortical bone exhibited the highest stress among all loading conditions. GTm demonstrated the highest stress (213.16 MPa), followed closely by GTg (212.98 MPa), while GZm (182.18 MPa) and GZg (181.88 MPa) exhibited lower stress values. Overall, the titanium implant groups showed higher cortical bone stresses than the zirconia implant groups, indicating that 45° oblique loading produced the most unfavorable cortical bone stress pattern.

Figure 3.16: Von misses stresses in the cortical bone under 90° oblique

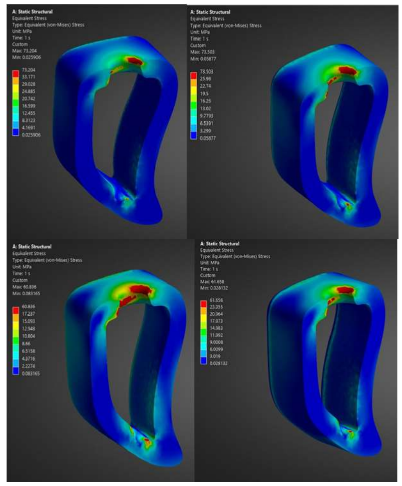

loading (225N)

Under 90° oblique loading (225 N), von Mises stress within the cortical bone decreased compared with 0° and 45° oblique loading but remained concentrated in the crestal cortical region. GTm exhibited the highest stress (73.503 MPa), followed by GTg (73.204 MPa), while GZm (61.658 MPa) and GZg (60.836 MPa) demonstrated lower stress values. The crestal cortical bone remained the principal site of stress concentration in all groups.

Overall, cortical bone demonstrated greater and more localized von Mises stress than cancellous bone, with maximum stress consistently concentrated in the crestal cortical bone adjacent to the implant neck under all loading conditions. The highest cortical bone stress was observed under 0° oblique loading in the titanium implant groups, with GTg (247.68 MPa) and GTm (247.39 MPa).

Von mises stress in cancellous bone

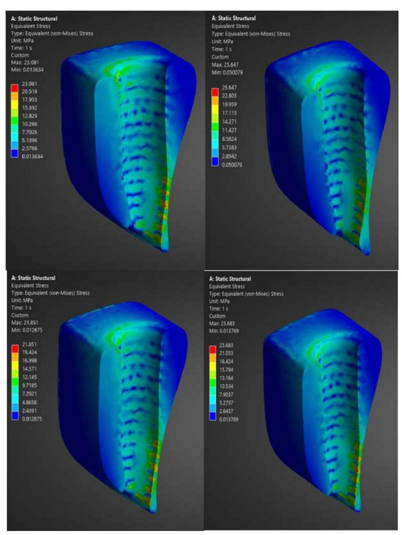

Figure 3.17: Von misses stresses in the cancellous bone under axial loading (600N)

Under axial loading (600 N), von Mises stress within the cancellous bone was lower and more diffusely distributed along the implant body than in the cortical bone. GTm exhibited the highest stress (25.647 MPa), followed by GZm (23.683 MPa), GTg (23.081 MPa), and GZg (21.851 MPa). Overall, cancellous bone demonstrated a more dispersed stress distribution than cortical bone.

Figure 3.18: Von misses stresses in the cancellous bone under 0° oblique loading (225N)

Under 0° oblique loading (225 N), von Mises stress within the cancellous bone decreased compared with axial loading and remained distributed around the implant threads and adjacent trabecular bone. GTm

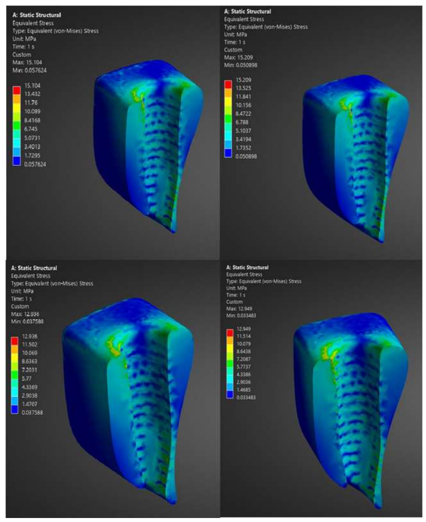

exhibited the highest stress (13.333 MPa), followed closely by GTg (13.283 MPa), while GZm (11.326 MPa) and GZg (11.281 MPa) demonstrated lower stress values. Overall, the titanium implant groups exhibited slightly higher cancellous bone stresses than the zirconia implant groups.

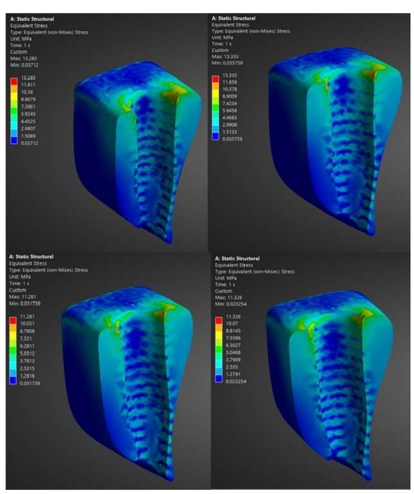

Figure 3.19: Von misses stresses in the cancellous bone under 45° oblique loading (225N)

Under 45° oblique loading (225 N), von Mises stress within the cancellous bone increased compared with 0° oblique loading. GTm exhibited the highest stress (15.209 MPa), followed by GTg (15.104 MPa), while GZm (12.949 MPa) and GZg (12.936 MPa) demonstrated lower and comparable stress values. Overall, the titanium implant groups exhibited slightly higher cancellous bone stresses than the zirconia implant groups.

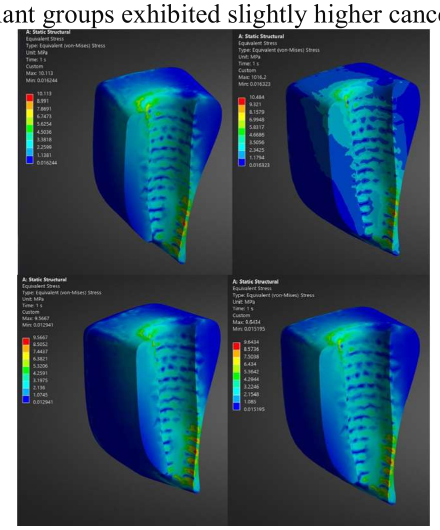

Figure 3.20: Von misses stresses in the cancellous bone under 90° oblique loading (225N)

Under 90° oblique loading (225 N), von Mises stress within the cancellous bone remained diffuse and lower than that observed in the cortical bone. GTm exhibited the highest stress (10.484 MPa), followed by GTg (10.113 MPa), while GZg (9.6436 MPa) and GZm (9.5667 MPa) demonstrated lower stress values. Overall, cancellous bone exhibited relatively low stress magnitudes in all groups under this loading condition.

Overall, **Figures 3.17 to 3.20** show that cancellous bone exhibited lower and more diffuse stress distribution than cortical bone under all loading conditions.

Discussion

The present three-dimensional finite element analysis evaluated the stress distribution in titanium and zirconia implants restored with monolithic zirconia and graphene crowns using standardized zirconia abutments under axial and oblique loading conditions. Biomechanical stress distribution is a critical determinant of the long-term success of implant-supported restorations, making the evaluation of different implant-restoration combinations clinically relevant.[5]

As occlusal forces are initially received by the crown, stress transmission through the implant-restoration complex begins at this level.[2] Comparable crown stress values were observed between titanium and zirconia implant groups restored with the same crown material (GTg vs GZg and GTm vs GZm), indicating that implant material had minimal influence on crown stress. This may be attributed to the standardized zirconia abutments used in all groups.[7] However, graphene crown groups consistently exhibited lower peak stresses and a more diffuse stress distribution than monolithic zirconia crown groups, reflecting the lower elastic modulus and greater resilience of graphene, which enables improved energy absorption and stress redistribution. These findings agree with those of Edward E. Daou et al., who reported greater localized stress accumulation in zirconia restorations, [12] Handan Yılmaz et al., who demonstrated higher stress concentration in rigid ceramic crowns, [13] and Alshamaa AA et al., who reported the superior mechanical properties of graphene-based restorations. [14]

Within the abutment-screw complex, maximum von Mises stress was consistently concentrated in the cervical region adjacent to the implant platform. Since zirconia abutments were standardized, the observed variations were primarily related to differences in implant and crown materials. Titanium implant groups demonstrated lower abutment stresses than zirconia implant groups under 0° and 45° oblique loading, which may be attributed to the lower elastic modulus of titanium and its greater capacity for elastic deformation. [11] Similar findings were reported by Saeed Al-Asaadi et al. [15] Furthermore, graphene crown groups consistently generated lower cervical abutment stresses than the corresponding monolithic zirconia crown groups owing to their improved stress dissipation.

Maximum implant stress was consistently concentrated at the crestal module, corroborating the findings of Himmlová et al., Geng et al., and Hariharan et al., who identified this region as the principal load-bearing area and the site most susceptible to marginal bone loss. [16,17,18] Zirconia implant groups exhibited higher internal implant stresses than titanium implant groups, which can be attributed to the higher elastic modulus and stiffness of zirconia. [53] In addition, monolithic zirconia crowns transmitted greater stresses to the implant than graphene crowns, whereas graphene restorations reduced stress concentration through improved energy absorption.[19] Loading direction also influenced stress distribution, with 45° oblique loading producing the highest implant stresses because of increased bending moments and shear forces. Similar observations were reported by Eskitascioglu et al. [20]

Stress was ultimately transferred to the peri-implant bone, where titanium implant groups demonstrated higher cortical bone stresses than zirconia implant groups, particularly under 0° and 45° oblique loading. Cortical bone consistently exhibited greater stress concentration than cancellous bone, with peak stresses localized at the crestal region adjacent to the implant neck. [8] The lower elastic modulus of titanium facilitates greater stress transfer to the surrounding bone, whereas the higher stiffness of zirconia retains more stress within the implant structure. [21] These findings are consistent with those of Pevida et al., who reported lower cortical bone stress but higher internal implant stress in zirconia implants, [22] as well as Sabiha Kouser et al. [8] and Merve Bankoglu Güngör and Handan Yılmaz. In contrast, cancellous bone demonstrated lower, more diffuse stress distribution, consistent with the observations of Holmes DC. [5,23]

Although graphene crown groups exhibited marginally lower cortical and cancellous bone stresses than monolithic zirconia crown groups, the differences were comparatively small, with GZg demonstrating the most favorable overall bone stress distribution.

Overall, the present findings demonstrate that both implant and restorative materials influence biomechanical stress distribution. Zirconia implants tended to retain greater stresses within the implant structure, whereas titanium implants transferred relatively higher stresses to the surrounding bone. In contrast, graphene crowns consistently reduced stress concentration within the crown, abutment, and implant while maintaining peri-implant bone stresses comparable to those of monolithic zirconia crowns. These findings suggest that graphene-based restorations may provide a biomechanical advantage, particularly under oblique loading conditions, and highlight the importance of selecting implant and restorative materials together to optimize load transfer and improve the longevity of implant-supported restorations. [24]

The findings of this study should be interpreted within the limitations of finite element analysis, including the assumption of homogeneous, isotropic, and linearly elastic material properties, idealized osseointegration, and the absence of fatigue or cyclic loading. Nevertheless, this study provides valuable insight into the biomechanical behavior of contemporary implant and restorative materials and provides a foundation for future in vitro and clinical investigations.

Conclusion

Within the limitations of this finite element study, both implant material and restorative material affected stress distribution within the implant-supported restoration. Zirconia implants developed higher internal implant stresses, whereas titanium implants transferred relatively greater stress to the surrounding bone. Graphene crowns demonstrated a more favorable stress distribution than monolithic zirconia crowns, indicating their potential as an alternative occlusal restorative material. Oblique loading, particularly at 45°, generated the highest stresses in all components, highlighting the critical influence of occlusal loading direction. Further in vitro and clinical investigations are recommended to validate these findings and determine their long-term clinical significance.

References

1. Sevimay M, Usumez A, Eskitascioglu G. The influence of various occlusal materials on stresses transferred to implant - supported prostheses and supporting bone: a three-dimensional finite-element study. J Biomed Mater Res B Appl Biomater. 2005;73B:140–147.
2. Gujjarlapudi MC, Nunna NV, Manne SD, Sarikonda VR, Madineni PK, Meruva RNR. Predicting peri-implant stresses around titanium and zirconium dental implants: a fini te element analysis. J Indian Prosthodont Soc. 2013;13(3):196–204.
3. Villabona Lopez CA, Amorin Vasco MA, Ruales E, Bedoya KA, Benfatti CM, Bezzon OL, et al. Three-dimensional finite element analysis of stress distribution in zirconia and titanium dental implants. J Oral Implantol. 2018;44:409–415.
4. Tretto PHW, dos Santos MBF, Spazzin AO, Pereira GKR, Bacchi A. Assessment of stress/strain in dental implants and abutments of alternative materials compared to conventional titanium alloy: 3D non-linear finite element analysis. Comput Methods Biomech Biomed Engin. 2020. doi: 10.1080/ 10255842.2020.1731481.
5. Bankoglu Güngör M, Yılmaz H. Evaluation of stress distributions occurring on zirconia and titanium implant -supported prostheses: a three- dimensional finite element analysis. J Prosthet Dent . 2016;116(3):346–355.
6. Choi SM, Choi H, Lee DH, Hong MH. Comparative finite element analysis of mandibular posterior single zirconia and titanium implants: a 3 - dimensional finite element analysis. J Adv Prosthodont. 2021; 13(6): 396 – 407.
7. Milone D, Fiorillo L, Alberti F, Cervino G, Filardi V, Pistone A, et al. Stress distribution and failure analysis comparison between zirconia and titanium dental implants. Procedia Struct Integr. 2022;41:680–691.
8. Kouser MS, Prathibha M, Altaher Mohammed OB, Elhammali NA, Saib Jameel A, Chauhan M, et al. A finite element analysis of peri - implant stresses surrounding zirconium and titanium dental implants. J Pharm Bioallied Sci. 2024;16(Suppl 4):S3377–S3379.
9. Ihde S, Goldmann T, Himmlova L, Aleksic Z. The use of finite element analysis to model bone- implant contact with basal implants. Oral Implantol (Rome). 2008; 1(2): 54–63.
10. Osman RB, Swain MV. A critical review of dental implant materials with an emphasis on titanium versus zirconia. Materials (Basel). 2015; 8(3): 932–58.
11. Eser A, Tonuk E, Akca K, Dard MM, Cehreli MC. Predicting time - dependent remodeling of bone around immediately loaded dental implants with different designs. Med Eng Phys. 2013;35(10):1427–35.
posterior mandibular bone. J Clin Med. 2026;15(1):104.
12. Daou EE. The zirconia ceramic: strengths and w eaknesses. Open

Dent J. 2014;8:33–42.
13. Yılmaz H, Aykent F, Doğan A. Evaluation of stress distributions in ceramic crown and supporting structures using finite element analysis. J Prosthodont. 2011;20(5):380–6.
14. Alshamaa AA, Al-Zahawi AR, Salloomi KN. Mechanical and optical properties of graphene-reinforced dental ceramic composites: a review. J Dent Mater Tech. 2022;11(3):120–9.
15. Al- Asaadi S, Romeed S, Dunne S. Finite element analysis of stress distribution in zirconia abutments paired with titanium versus zirconia implants. J Prosthodont Res. 2025;69(1):45–53.
16. Himmlová L, Dostálová T, Kácovský A, Konvičková S. Influence of implant length and diameter on stress distribution: a finite element analysis. J Prosthet Dent. 2004;91(1):20–5.
17. Geng JP, Tan KB, Liu GR. Application of finite element analysis in implant dentistry: a review of the literature. J Prosthet Dent. 2001;85(6):585–98.
18. Hariharan A, Rathee M, Bhoria M, Bansal V, Gupta R. Stress distribution patterns around dental implants: a three - dimensional finite element analysis. J Oral Biol Craniofac Res. 2024;14(2):198–205.
19. Saberian M, Gonzalez C, Bravo M, Carvajal JC, Revuelta-Jiménez A.

Comparative finite element analysis and bone remodeling prediction of one- piece implants made of titanium, zirconia, PEEK, CFR- PEEK and GFR- PEEK. Materials (Basel). 2022; 15(3): 1142.
20. Eskitascioglu G, Usumez A, Sevimay M, Soykan E, Unsal E. The influence of occlusal loading location on stresses transfer red to implant-supported prostheses and supporting bone: a three - dimensional finite element study. J Prosthet Dent. 2004;91(2):144–50.
21. Talmazov G, Veilleux D, Abdulmajeed A, Bencharit S. Three - dimensional finite element analysis of stress distribution in peri - implant bone using CBCT-based model: comparison of one-piece yttria- stabilized zirconia and titanium implants. J Prosthodont. 2020;29(9):786–93.
22. Pérez-Pevida, E., Brizuela-Velasco, A., Chávarri-Prado, D., Jiménez-Garrudo, A., Sánchez-Lasheras, F., Solaberrieta-Méndez, E., Diéguez-Pereira, M., Fernández-González, F. J., Dehesa-Ibarra, B., & Monticelli, F. (2016). Biomechanical consequences of the elastic properties of dental implant alloys on the supporting bone: Finite element analysis. *BioMed Research International*, *2016*(1), 1850401.
23. Holmes DC, Loftus JT. Influence of bone quality on stress distribution for endosseous implants. J Oral Implantol. 1992; 23(3): 104–11.
24. Villabona Lopez CA, Suárez PA, Peña FM, Ávila JE. Three - dimensional finite element analysis of stress in peri - implant bone of titanium and zirconia dental implants under axial and oblique loading. J Oral Implantol. 2018; 44(3):175–82.